Geotech Geol Eng
https://doi.org/10.1007/s10706-019-00815-2

TECHNICAL NOTE

Petrophysical Properties of Opalinus Clay Drill Cores Determined from Med-XCT Images

Lukas M. Keller · Silvio B. Giger

Received: 29 October 2018 / Accepted: 9 January 2019

Abstract The determination of petrophysical properties such as density, porosity and mineralogical composition of the rock are key objectives in cored sections of drilling campaigns. In view of the large amount of sample material that accumulates during a drilling campaign, a seamless determination of the properties along the cores is not feasible if only direct methods are used. Therefore, fast, non-destructive and affordable methods have been developed. Three-dimensional images of Opalinus Clay drill cores were acquired by using a medical X-ray computed tomographic scanner (med-XCT). The CT numbers of the images were density calibrated, which allowed to determine bulk density variations along drill cores. Then, a relationship between rock composition and bulk density was built in form of linear regression models to predict the porosity or the contents of major components from density calibrated image data. This relationship was established on the basis of rock samples, of which mineralogical compositions and porosities were measured in the laboratory. It turned out that the bulk density of Opalinus Clay is systematically related to porosity and the contents of clay minerals, quartz and calcite. With increasing density, porosity and clay minerals content decrease. This is because the pores and clay minerals together form the porous clay matrix and are thus structurally connected. The density of the porous clay matrix is comparatively low, and its content therefore controls the bulk density of Opalinus Clay. With a decrease in the content of the porous clay matrix, the calcite and quartz contents both increase, which is associated with an increase in bulk density. No systematic behavior was found for the accessories. Thus, their influence on bulk density is considered to be small. Med-XCT in combination with reference samples allows the determination of the rock composition and porosity along drill cores. In the case of Opalinus Clay, a larger number of reference samples ($> \sim 50$) are required to predict the properties with confidence.

Keywords Medical X-ray tomography · Shale density · Shale composition · Opalinus Clay

1 Introduction

Med-XCT is a non-destructive method that can examine a large number of cores along their entire length in a short time. Med-XCT provides qualitative information (image contrast) about the density variation along drill cores, provided that the density variations are sufficiently large (Mees et al. 2003).

L. M. Keller (✉)
ZHAW, University of Applied Sciences, Wildbachstrasse 21, 8401 Winterthur, Zurich, Switzerland
e-mail: kelu@zhaw.ch

S. B. Giger
National Cooperative for the Disposal of Radioactive Waste, Wettingen, Switzerland

Published online: 13 January 2019

To this date this method was extensively applied to geomaterials (e.g. Ashi 1995, 1997; Mees et al. 2003; Taud et al. 2005; Jovanovic et al. 2013; Gupta et al. 2018). Since qualitative information in form of image grey values is not satisfactory, previous studies calibrated the grey values in order to obtain a quantitative density distribution in the geomaterials (Ashi 1995; Gupta et al. 2018). Regarding clay rocks the resolution of med-XCT is too low to resolve the individual pores or mineral grains, and the grey value of each resolution unit, the so-called voxel, reflects a bulk density, which is controlled by the local composition. Attempts were made to break down this bulk density into its individual summands (e.g. product between volume fraction and density of a certain mineral) in order to obtain information on porosities and mineral content (Gupta et al. 2018). Without further assumptions and provided that the densities of the individual components are known, the volume fractions in a two-component system are clearly determined for any given value of bulk density. For example, the porosity and volume fraction of the solid of each voxel can be determined in case the image data is density calibrated (Gupta et al. 2018). For more than two components the volume fractions are not clearly determined and in this case information of the dependence between bulk density and the volume fractions of the individual components is required. Such information can be obtained from rock samples for which the density and rock mineralogical composition was measured in the laboratory.

In this study we collected such data to explore a possible systematic relationship between density and composition. The key step is by assigning a composition to a given density value, which allows to calculate the composition distribution of entire drill cores based on the density-calibrated XCT image data. The investigated material is Opalinus Clay, a Jurassic shale designated as host rock for radioactive waste in Switzerland (Nagra 2002). For comparative site evaluation of a future repository several deep boreholes will be drilled in north-eastern Switzerland between 2019 and approximately 2021. The med-XCT method is already routinely used by Nagra to assess Opalinus Clay integrity of conditioned cores prior to shipment to laboratories for geomechanical testing (Giger et al. 2018). As the variability in the mineralogical composition of the host rock is considered one relevant aspect for site evaluation, it was decided to extend the med-XCT method for quantitative assessment of the mineralogical composition.

2 Samples and Applied Methods

The majority of the examined drill cores were taken from the Opalinus Clay unit at the Mont Terri rock laboratory, Switzerland (Bossart and Thury 2008). The rock laboratory is in and alongside the security gallery of the Mont Terri motorway tunnel in north-west Switzerland. At the Mont Terri site, the Opalinus Clay can be subdivided into three main facies: shaley facies, sandy facies and carbonate rich sandy facies. The samples are all taken about 250 m below the surface. The shaley facies of Opalinus clay typically contains about 60–70 wt% clay minerals, 10–20 wt% carbonate minerals, 10–20 wt% quartz and accessory constituents such as feldspars, pyrite and organic carbon. The sandy facies is substantially lower in clay minerals ($\sim$ 30–40 wt%) and contains about 40–50 wt% carbonate minerals and 20–30 wt% quartz (Nagra 2002). In addition to the sample taken from Mont Terri, some samples were taken from a shallow borehole (depth of extraction 22–70 m below ground) near the town of Lausen, Switzerland. Immediately after extraction from the ground, all cores were first wrapped in aluminum foil and sealed under vacuum, then conditioned in a PVC core barrel by filling the annulus with a fast-curing resin (Giger et al. 2018).

2.1 Whole Rock Mineralogy and Petrophysical Measurements

We compiled a data set consisting of bulk rock densities and related mineral compositions that were measured in the laboratory. Thereby, the sample localities are well known along the drill cores (see below). The CT-values corresponding to the densities and rock compositions could thus be extracted from the image data. For some samples no CT-values could be determined because of the lack of image data. These samples were used to increase the size of the data set that was used to establish the relationship between density and mineralogical composition (see below). The whole rock mineralogy and the densities were measured by the Rock–Water Interaction group of the University of Bern, Switzerland. Details of the measurement procedure can be found in Mazurek et al.

(2012). In summary: the mineralogical compositions of the samples were measured by X-ray diffractometry. Porosity is a water loss porosity that was calculated from the measured change in weight during drying of the samples at 105 degrees until reaching a constant weight. The bulk-wet density was measured using the paraffin displacement method that is based on the Archimedes principle.

2.2 Imaging

The Opalinus Clay drill cores were imaged using a medical XCT. The cores were scanned using always the same instrument set up. Imaging was performed with a Somatom Definition AS 64 (Siemens, Forchheim, Germany). The tube voltage was 140 kV. All scans were performed using the automatic dose modulation software (CARE Dose 4D, Siemens, Forchheim, Germany). Collimation was 64×0.6 mm. All image reconstructions were performed using the soft tissue kernel (I31f). The investigated samples had diameters of about 12 cm and the lengths of the whole cores were scanned. This volume in combination with the used XCT device yielded image data with a voxel size of $0.25 \times 0.25 \times 0.4$ mm.

XCT is an imaging method where the image resolution is linked to sample size and on the length scale of meters the expected voxel size (i.e. resolution) is on the hundreds of micrometers. This length is much larger when compared to typical grain and pore sizes in clay rocks. Hence, the gray-value of certain image voxel visualizes a "mean" material density, which is related to the volume fractions of different minerals filling the volume of that particular voxel. Because the porous clay matrix is comparable low in density, dark parts in the images are expected to be clay-rich, whereas the brighter regions are expected to be carbonate-rich (see below).

2.3 Basic Information on XCT Technology

The incident X-ray intensity varies as function of the X-ray path length and the linear attenuation coefficient (LAC) of the target material. The LAC is a function of the chemical composition and the density of the target material. Grey levels in XCT images represent attenuation in each pixel. Grey levels in XCT images are scaled according to the Hounsfield (HU) scale, where air has HU = − 1000 and water has HU = 0. The XCT device used is calibrated daily for air. The Hounsfield scale is defined as:

$$HU = \frac{\mu_{object} - \mu_{water}}{\mu_{water} - \mu_{air}} \cdot 1000, \quad (1)$$

where μ is the LCA of the respective material.

2.4 Beam Hardening Correction

Beam hardening (BH) is a phenomenon that is associated with the polychromatic nature of the X-ray beam of the used med CT instrument. When such X-rays travel through a dense homogenous material, the X-rays with lower energy are preferentially absorbed to those X-rays with higher energy levels. Hence, the beam spectrum is successively depleted at the lower energy spectrum as it passes through the material. As a result, the spectrum of the X-ray beam "hardens" and becomes less attenuated further in a homogenous material. Because of these non-linear effects, attenuation in a homogenous rock material is not proportional to density along a cross-section through a cylindrical shaped and homogenous core sample. Consequently, the reconstructed XCT images typically show a higher attenuation (i.e. higher CT numbers) at the outer region when compared to the inner part of the rock core even in the supposed case that the rock core is composed of a single mineral phase. Among other problems, the presences of BH artifacts therefore cause problems if the density of the material is determined from density calibrated XCT images. Without the correction of BH artifacts there is a difference between a density measure at the rim and in the center of the core, whereas the density measure in the core underestimates the true density value. Several methods, which either modify the XCT instrument or improve the software, have been developed to eliminate the BH artifacts. This includes physical pre-filtering to pre-harden the X-ray photon spectrum, the dual energy approach, and a variety of computational pre- and post-processing image corrections (Schlüter et al. 2014). The major drawback of computational methods that attempt to the eliminate BH artifacts during pre-processing is that they often rely on known material properties of the investigated sample or unknown values of adjustable parameters (Brabant et al. 2012; Khan et al. 2016). For example, the often-required knowledge of the number and

distribution of phases and the corresponding attenuation coefficients is generally not available prior to the investigations. BH correction methods, which are applied after classical image reconstruction, involve fitting a surface to the 2D grey level distribution represented by the individual images of the XCT image stack. The corrected image is then the difference between the surface and the original grey level image (Khan et al. 2016). In this study we employ a similar approach. From visual inspection of image slices perpendicular to the cylinder axis it is apparent that the reconstructed CT numbers depend on the radial distance from the center of circular sample (Fig. 1).

Thereby, the CT numbers systematically decrease towards the center of the sample. Hence, the beam-hardening artifact is considered as a radial function. To remove the BH artifact, the radial distance between the rim and the center of the cylindrical sample was calculated for all pixels, which yielded a distribution of CT numbers as a function of the radial distance (Fig. 2). Then, a second-degree polynomial function p(r) was fitted to these data (Fig. 2). The beam hardening correction is then a radial function that is given by the difference p(0)–p(r) (Fig. 2). The corrected image (Fig. 1c) was then obtained by adding the respective correction value to the grey values of the pixels. The distribution of correction values related to the XCT image depicted in Fig. 1a is shown in Fig. 1b. This procedure is applied to each slice of the image stack.

The method was applied to a whole image stack and a cross-section through the center and parallel to the core axis was constructed. Figure 3 shows the cross-sections prior and after BH correction. The visual inspection shows that the method satisfactorily removes the darker areas along the core axis. The artifact was removed from all scans (including the image data related to the calibration phantom) in this way.

3 Density Calibration of CT Numbers

In this chapter we attempt to density calibrate the CT numbers of the XCT images in order to obtain an overview of the real density distribution along drill cores. As input we use data related to a so-called density calibration phantom as well as measured rock densities, which were determined in the laboratory.

3.1 Input 1: Density Calibration Phantom

In order to obtain a relation between image CT numbers given in units of HU and the density of the target material, the used XCT instrument is equipped with a bone density calibration phantom, which is built into the table and is scanned along with the samples (Fig. 4, Table 1).

The calibration phantom was scanned with the same XCT instrument and with the same settings as all the other core samples. Then, the CT numbers of the

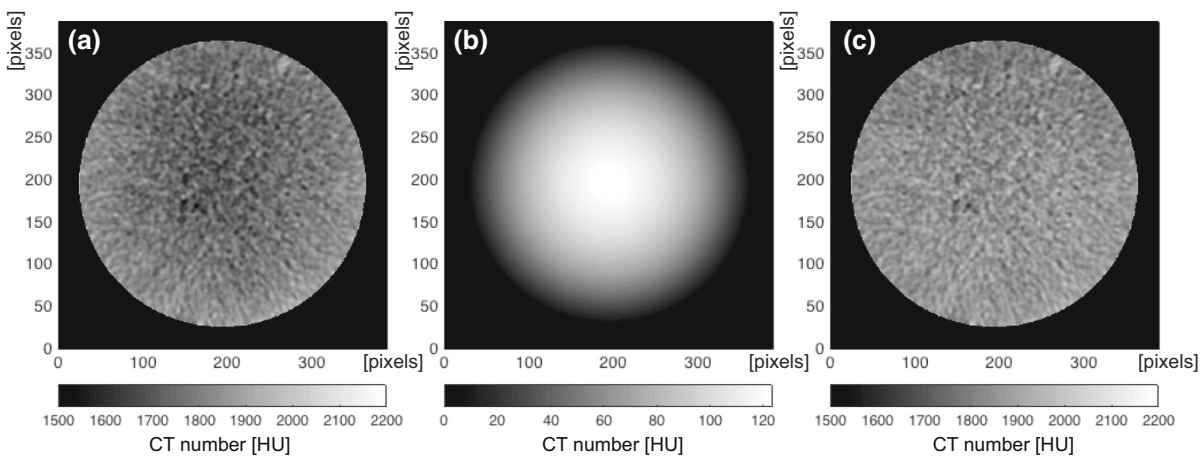

Fig. 1 **a** XCT image showing the original grey value distribution of an XCT image. **b** Beam hardening correction that was added to original XCT image (see also Fig. 2). **c** Corrected XCT image

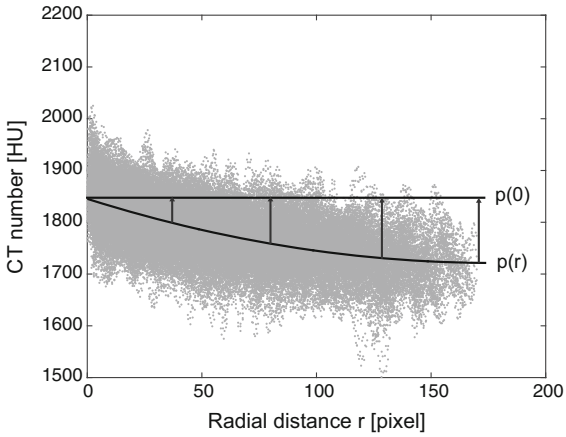

Fig. 2 Presentation of the method used to correct the beam-hardening artifact. A second-order polynomial function was adapted to the radial distribution of the gray values. The gray value distribution shown corresponds to the image shown in Fig. 1a. The radial beam hardness correction was then taken as the difference p(0)–p(r)

materials with known densities were measured (Table 1). In addition to the rock densities that were measured in the laboratory (see below), these relationships between the densities and the CT numbers were used to establish a linear relationship between the CT number and the density. Because the instrument is calibrated to air, we also included CT number/density relation of air (− 1000 HU/0.0012 g/cm^3) into the data set to establish the linear relation.

3.2 Input 2: Measured Rock Densities

Rock densities were measured at the University of Bern, Switzerland (see above). The sampling procedure was as follows. The cores were XCT scanned and sample localities with different HU values were selected using a profile showing the average HU values in the individual image planes (Fig. 5). The sample locations were measured and the dimensional sketch was handed over to the laboratory together with the core. The core was then sawn exactly according to this plan and composition and densities were determined for these sample volumes. The mean HU values were then also determined exactly for these sample volumes. The result is a data set consisting of measured densities and the corresponding HU values Table 2.

This data was used to perform a linear regression and assess the relationship between CT numbers and

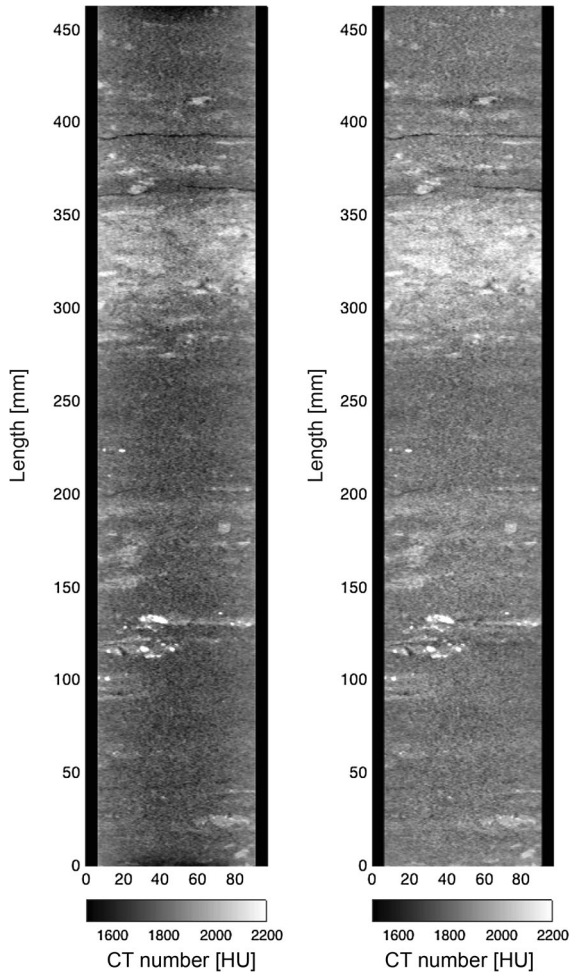

Fig. 3 Cross-sections parallel to the core axis of an Opalinus Clay drill core. Left: XCT image prior to BH correction. Note, the BH artifacts are manifested in form of a dark area in the central part of the image. Right: Corrected XCT image

rock densities as shown on Fig. 6. The quality of the linear fit is good and the prediction of the mean density is acceptable. To evaluate the prediction capabilities of expected values related to future samples, we calculated the tolerance interval according to Wallis (1951). As an example, the interval (green lines in Fig. 6) suggests that one can be 95% sure (confidence) that the interval contains 95% of the values of future samples. Setting the confidence to 50% corresponds to the usual prediction interval. The size of the tolerance interval is considerable, which is mainly due to the low number of available samples. To improve the prediction quality, the number of samples will be further increased.

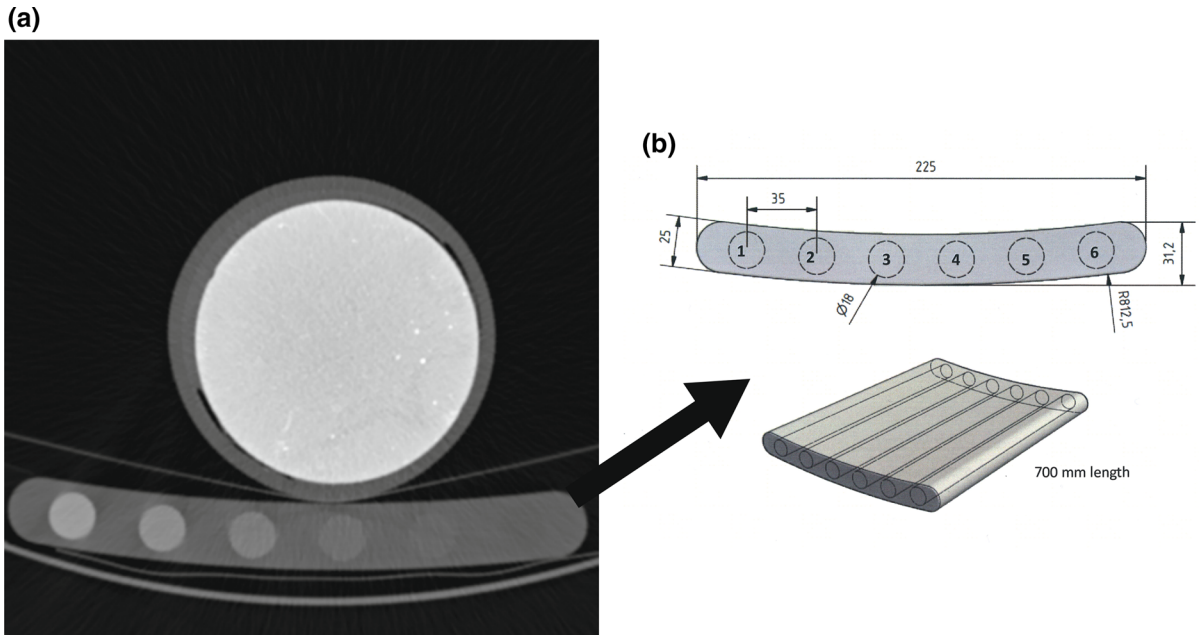

Fig. 4 **a** XCT image showing a cross-section through a clay rock core and the calibration phantom. **b** Technical drawings of the calibration phantom. The lengths are all in units of millimeter

Table 1 Density of the materials, which are inserted into the calibration phantom depicted in Fig. 4

Insert #	Density (g/cm^3)	CT numbers (HU)
1	1.56 ± 0.02	858
2	1.42 ± 0.02	634
3	1.28 ± 0.02	416
4	1.15 ± 0.02	206
5	1.08 ± 0.02	95
6	1.02 ± 0.02	− 16

4 Prediction of Modal Mineralogy and Porosity from Given Density Values

Med-XCT is an efficient method to determine density variations along drill cores. It would be a decisive improvement of the method if additional information such as porosity and rock composition could be obtained from the densities determined from XCT images. What we know from the image data is the bulk density of the component mixture for each volume unit of voxel. The problem at hand is thus the determination of the volumetric contents of each component (modal mineralogy) and porosity for a given density.

The following two-stage approach was chosen for this purpose. First the bulk density is calculated for samples with known compositions and porosity. Because the measured mineral composition of samples in the available data set is given in units of wt% they must be transferred into units of vol%, which requires the knowledge of the density of the individual minerals. The use of calculated densities increases the number of available samples because the density was not measured for all samples. Increasing the number of samples improves the prediction quality. As then shown, the difference between calculated and measured densities is minor (Table 2). Preference was also given to a relationship between composition and density and not between composition and CT numbers, as the sample location is not known with sufficient accuracy for all samples and thus, the CT number cannot be determined for all samples.

The second step involves performing a linear regression to establish the relation between density and volumetric contents of the components and porosity.

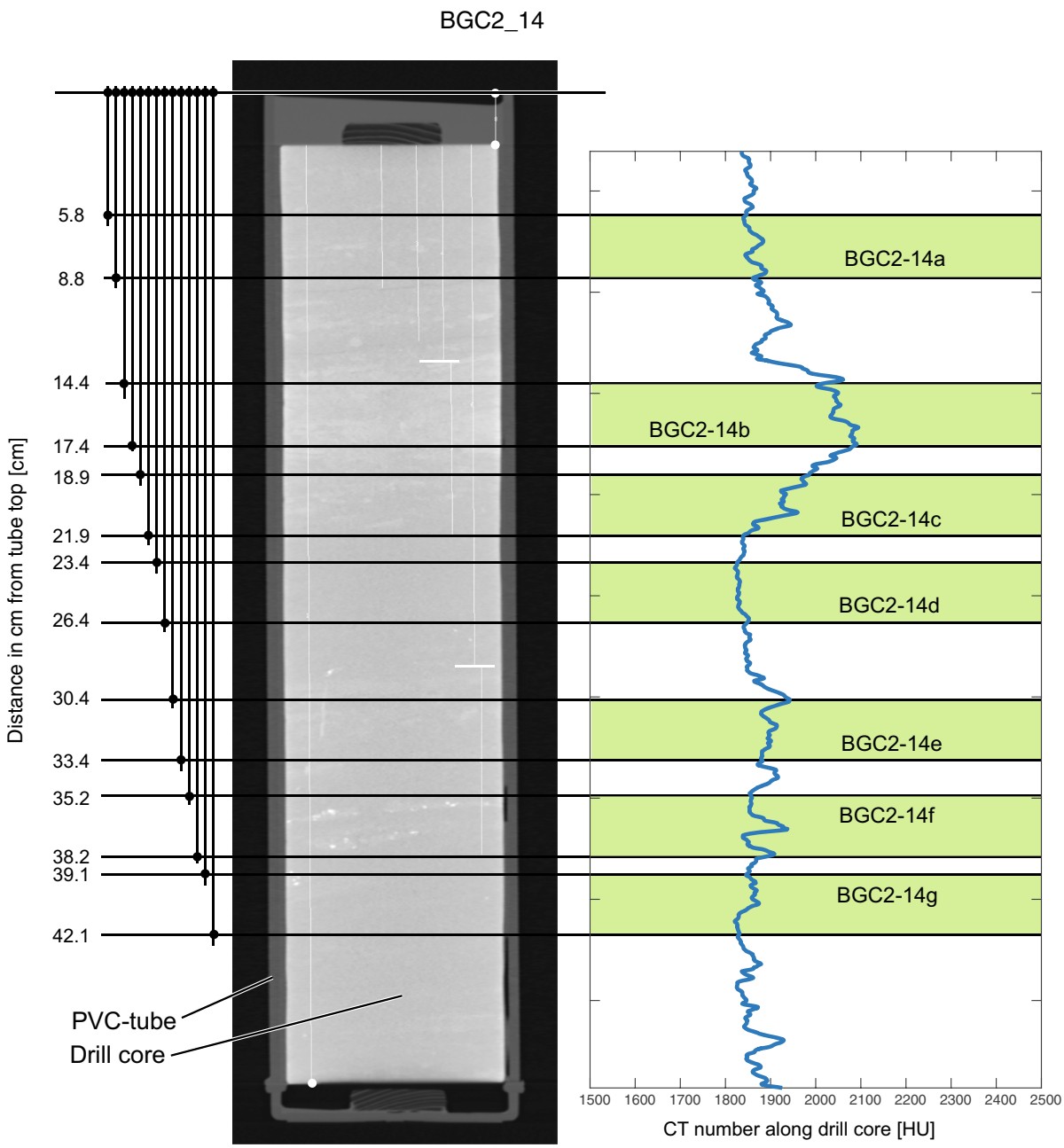

Fig. 5 Dimensional sketch for the core BGC2-14 with marked sample locations (green)

4.1 On the Density of Clay Minerals in Opalinus Clay

The problem that arises is that the density of the clay minerals is poorly known. To overcome this problem, the clay mineral density was determined based on a collection of samples, of which grain density and rock composition are known (Tables 2, 3). Thereby, the clay mineral density was varied until the difference between measured and calculated grain density was minimized. The density of other minerals (Qtz = 2.65, Fsp = 2.62, CC = 2.72, Dol = 2.84, Ank = 3.05, Pyr = 5.02, Sid = 3.96, C(org) = 1.30 all values in units of g/cm^3) was held constant. The smallest

Table 2 Compilation of data related to Opalinus Clay samples, which were used in this study to density calibrate the CT numbers of the image data

Locality	Sample	Calculated grain density (g/cc)	Calculated bulk density (g/cc)		Measured grain density (g/cc)	Measured bulk density (g/cc)	CT Number (HU)
Lausen	3.00	2.69	2.39				1858
Lausen	8.00	2.69	2.47				1894
Lausen	9.00	2.69	2.45				1886
Lausen	11.00	2.69	2.41				1867
Lausen	12.00	2.72	2.46				1868
Lausen	13.00	2.67	2.38				1818
Lausen	13.00	2.67	2.38				1818
Mont Terri	1-0	2.68	2.49		2.69	2.49	–
Mont Terri	1-45	2.69	2.53		2.70	2.55	–
Mont Terri	1-90	2.69	2.48		2.71	2.51	–
Mont Terri	2-0	2.69	2.45		2.69	2.46	–
Mont Terri	2-45	2.69	2.48		2.70	2.48	–
Mont Terri	2-90	2.68	2.46		2.69	2.47	–
Mont Terri	3-0	2.70	2.41		2.68	2.46	–
Mont Terri	3-45	2.70	2.42		2.69	2.45	–
Mont Terri	3-90	2.70	2.42		2.68	2.44	–
Mont Terri	4-0	2.69	2.41		2.69	2.45	–
Mont Terri	4-45	2.70	2.43		2.69	2.46	–
Mont Terri	4-90	2.70	2.43		2.69	2.45	–
Mont Terri	BGC2-14A	2.68	2.46		2.70	2.47	1861
Mont Terri	BGC2-14B	2.69	2.55		2.70	2.54	2060
Mont Terri	BGC2-14C	2.68	2.47		2.70	2.47	1914
Mont Terri	BGC2-14D	2.68	2.45		2.69	2.45	1832
Mont Terri	BGC2-14E	2.68	2.43		2.70	2.47	1885
Mont Terri	BGC2-14F	2.67	2.47		2.70	2.46	1876
Mont Terri	BGC2-14G	2.68	2.44		2.70	2.44	1837
Mont Terri	BGC2-34	2.70	2.43		2.76	2.48	1845
Mont Terri	BGC2-34	2.70	2.44		2.69	2.43	1842
Mont Terri	BGC2-34	2.69	2.44		2.70	2.44	1842
Mont Terri	BGC2-34	2.71	2.44		2.69	2.42	1853
Mont Terri	BGC2-19	2.69	2.54		2.69	2.54	1919
Mont Terri	BGC2-19	2.71	2.60		2.70	2.59	2105
Mont Terri	BGC2-31	2.70	2.43		2.72	2.45	1841
Mont Terri	BGC2-31	2.70	2.44		2.72	2.45	1842
Mont Terri	BGC2-31	2.70	2.45		2.70	2.45	1841
Mont Terri	BGC2-18	2.69	2.51		2.69	2.51	1933
Mont Terri	BGC2-18	2.68	2.49		2.69	2.49	1865
Mont Terri	BGC2-17	2.68	2.49		2.69	2.49	1871
Mont Terri	BGC2-15-1-oben	2.70	2.43		2.69	2.41	1882
Mont Terri	BGC2-15-1-unten	2.71	2.50		2.71	2.48	1977
Mont Terri	BGC2-15-2-oben	2.69	2.42		2.69	2.40	1884
Mont Terri	BGC2-15-2-unten	2.71	2.45		2.70	2.44	1929
Mont Terri	1756_BGC2_17_01	2.67	2.59	X	2.65	2.60	2104

The table shows the coincidence between measured and calculated densities. The table presents bulk density of samples used to assess the relationship between bulk density and composition. The "density" vector x is the second column in matrix X

difference for the whole data set was obtained for a clay mineral density of 2.73 g/cm^3. Table 2 documents the difference between measured and calculated density.

4.2 Relation Between Bulk Density and Composition

The wet bulk density related to a mixture consisting of several constituents may be given as

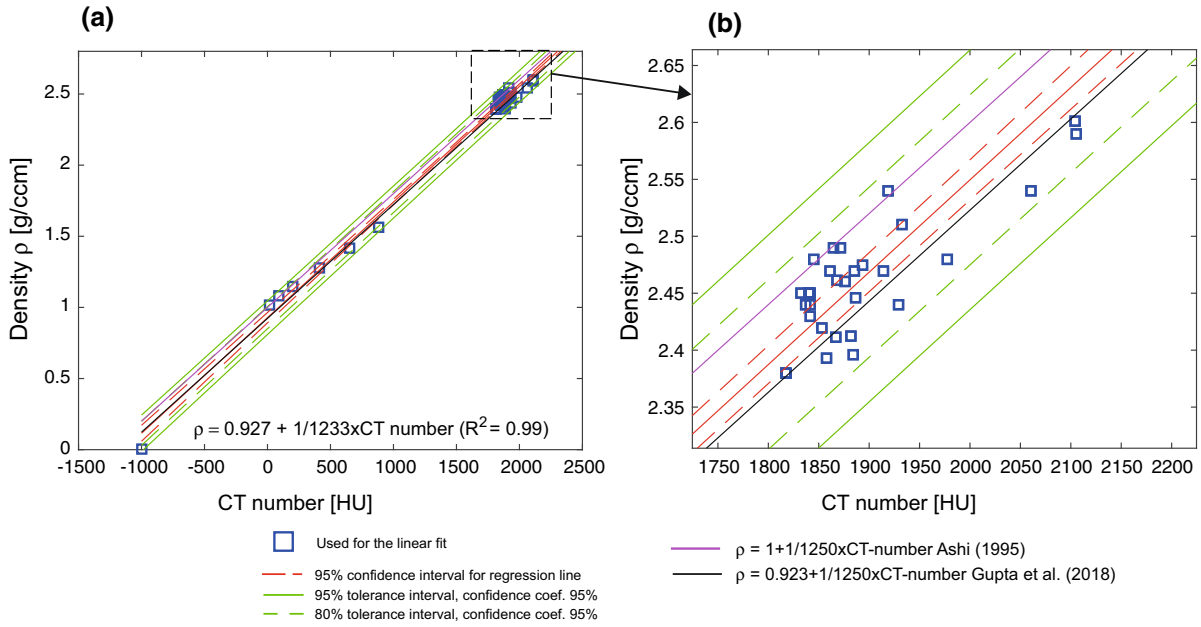

Fig. 6 **a** and **b** Show the linear fit between CT numbers and density. **b** Is an enlargement of the marked area. The meaning of the symbols and red and green lines is shown below the plots

$$\rho_{wet} = \frac{\sum_{i=1}^{d} m_i}{\sum_{i=1}^{d} V_i} \tag{2}$$

where m_i is the mass of the i'th constituent and V_i the related volume of the respective constituent. Expression (2) can be rewritten as

$$\rho_{wet} = \sum_{i=1}^{d} \rho_i \phi_i \tag{3}$$

where ϕ_i is the volume fraction of the ith constituent and ρ_i is the known density of the respective constituent. The calculation of the modal mineralogy from the multivariable Eq. (3), on the assumption that the bulk density is known (e.g. from XCT analysis) is impossible because the equation involves several independent variables even if we consider that the volume fractions of the constituents sum up to one.

To overcome this problem, it is reiterated that the aim is to predict the modal mineralogy and porosity for a given value of bulk density, which in turn was obtained from the density-calibrated CT numbers. Hence, the density is considered as the independent variable and the different volume fractions of the constituents are considered as the response variables. The linear regression model that was fitted to the data had thus the following form:

$$\begin{bmatrix} y_{11} & y_{12} & \cdots & y_{1d} \\ y_{21} & y_{22} & \cdots & y_{2d} \\ \vdots & \vdots & \vdots & \vdots \\ y_{n1} & y_{n2} & \cdots & y_{nd} \end{bmatrix} = \begin{bmatrix} 1 & x_{11} \\ & x_{21} \\ \vdots & \vdots \\ 1 & x_{n1} \end{bmatrix} \begin{bmatrix} \beta_{01} & \beta_{02} & \cdots & \beta_{0d} \\ \beta_{11} & \beta_{12} & \cdots & \beta_{1a} \end{bmatrix} + \begin{bmatrix} \varepsilon_{11} & \varepsilon_{12} & \cdots & \varepsilon_{1d} \\ \varepsilon_{21} & \varepsilon_{22} & \cdots & \varepsilon_{2d} \\ \vdots & \vdots & \vdots & \vdots \\ \varepsilon_{n1} & \varepsilon_{n2} & \cdots & \varepsilon_{nd} \end{bmatrix} \tag{4}$$

where the responses in Y (Table 3) are the volume fractions of d = 10 constituents. Data exists for N = 43 different samples. The predictors in the column vector x are the known bulk densities of the N samples (Table 2). In order to include a constant term in the regression a column vector of ones was added to matrix X. The beta matrix contains 2 × d regression coefficients: d intercept terms and d slope terms (Table 4). E is the matrix of residuals.

As can be seen from Table 4, comparatively higher coefficients of determination R^2 were obtained for the linear relationships between density and: (1) porosity, (2) calcite and (3) clay minerals. Regarding minerals with volumetric contents of a few percent the linear models are poor, which in turn suggest the lack of a systematic relation between bulk density and these

minerals. Therefore, the linear models, which refer to the minerals with low content, were not further evaluated. An exception was made for quartz. Even if the linear model seems poor for quartz, it has been further investigated because quartz is one of the three main components of Opalinus Clay (cf. Sect. 2).

Linear models are based on assumptions, such as the normal distribution of errors in the observed

Fig. 7 **a**, **c**, **e** and **g** (left column) Shows the normal probability ▶ plots of the residuals related to the linear regression models for the relationship between density and minerals or pores. The circles mark the excluded data points. **b**, **d**, **f** and **h** (right column) Shows the linear models (red lines) for the relationship between density and minerals or pores. The meaning of red and red and green lines is shown below the plots

Table 3 Compilation of data related to Opalinus Clay samples, which were used in this study to density calibrate the CT numbers of the image data

Locality	Sample	Calcite (vol%)	Dolomite (vol%)	Siderite (vol%)	Quartz (vol%)	Albite (vol%)	K-Fsp (vol%)	Pyrite (vol%)	C(org) (vol%)	Clay minerals (vol%)	Porosity (vol. %)	
Lausen	3.00	6.19	1.32	1.42	18.39	0.85	2.54	0.09	1.86	49.57	17.80	
Lausen	8.00	9.65	1.23	0.27	29.21	0.90	4.48	0.37	1.07	39.94	12.90	
Lausen	9.00	4.82	1.32	0.47	27.80	1.32	3.51	0.14	1.20	45.02	14.40	
Lausen	11.00	5.44	1.16	0.33	22.89	0.86	3.00	0.23	1.59	48.09	16.40	
Lausen	12.00	4.06	1.95	3.07	17.45	0.88	2.21	0.63	1.56	53.20	15.00	
Lausen	13.00	2.74	0.87	0.17	10.81	0.84	1.68	0.69	1.73	62.88	17.60	
Lausen	13.00	2.28	0.73	0.17	9.98	0.84	1.26	0.66	1.75	64.74	17.60	
Mont Terri	1-0	14.58	3.07	0.24	33.89	3.23	3.55	0.09	1.14	28.81	11.39	
Mont Terri	1-45	29.81	2.31	0.45	31.10	2.07	2.93	0.06	0.83	21.07	9.37	
Mont Terri	1-90	10.74	5.92	0.48	33.10	3.10	3.34	0.11	1.07	29.42	12.72	
Mont Terri	2-0	6.73	2.37	0.37	28.67	2.46	2.66	0.36	1.27	40.94	14.16	
Mont Terri	2-45	6.83	5.36	0.25	41.70	2.70	0.96	0.29	1.12	28.32	12.48	
Mont Terri	2-90	6.49	2.03	0.48	31.76	2.32	3.65	0.17	1.29	38.50	13.31	
Mont Terri	3-0	4.21	1.32	0.27	18.32	1.49	1.60	0.45	1.53	53.53	17.28	
Mont Terri	3-45	4.56	1.44	0.46	17.91	1.23	1.18	0.44	1.54	54.82	16.42	
Mont Terri	3-90	4.05	1.57	0.17	18.32	1.59	1.48	0.48	1.63	54.40	16.31	
Mont Terri	4-0	4.13	1.46	0.36	16.45	1.39	1.44	0.21	1.63	56.13	16.80	
Mont Terri	4-45	4.73	1.42	0.35	18.66	1.63	1.94	0.42	1.54	53.59	15.72	
Mont Terri	4-90	4.09	1.43	0.38	16.32	1.38	1.43	0.41	1.70	56.94	15.92	
Mont Terri	BGC2-14A	7.13	1.66	0.80	34.40	3.50	5.60	0.12	1.39	32.16	13.24	
Mont Terri	BGC2-14B	34.95	0.48	0.64	34.65	3.04	3.90	0.16	0.50	12.99	8.69	
Mont Terri	BGC2-14C	15.54	0.36	0.78	37.87	3.21	5.18	0.15	1.05	23.40	12.47	
Mont Terri	BGC2-14D	7.65	0.32	0.69	37.42	4.00	6.34	0.10	1.15	28.81	13.53	
Mont Terri	BGC2-14E	14.50	0.51	0.76	44.77	3.38	5.33	0.08	0.71	15.05	14.90	
Mont Terri	BGC2-14F	13.02	0.75	0.69	45.37	3.52	5.14	0.10	0.99	18.21	12.23	
Mont Terri	BGC2-14G	6.81	0.24	0.79	37.68	3.70	5.84	0.30	1.24	29.24	14.17	
Mont Terri	BGC2-34	6.94	1.09	0.47	15.45	1.79	1.88	0.41	1.63	54.56	15.79	
Mont Terri	BGC2-34	5.63	1.14	0.41	16.22	1.73	1.35	0.32	1.72	56.23	15.26	
Mont Terri	BGC2-34	5.05	1.66	0.43	17.00	2.78	1.62	0.40	1.92	54.04	15.11	
Mont Terri	BGC2-34	7.19	0.81	0.57	11.06	1.65	1.24	0.43	1.75	59.48	15.83	
Mont Terri	BGC2-19	10.48	6.55	1.07	46.62	3.91	3.27	0.09	1.16	18.02	8.83	
Mont Terri	BGC2-19	43.43	0.17	1.72	30.01	3.03	1.55	0.02	0.52	12.99	6.56	
Mont Terri	BGC2-31	10.64	0.43	0.34	16.56	2.90	3.21	0.52	1.56	48.22	15.60	
Mont Terri	BGC2-31	8.41	0.52	0.51	15.89	2.80	2.27	0.49	1.48	51.86	15.75	
Mont Terri	BGC2-31	8.55	0.63	0.47	15.08	2.47	1.99	0.50	1.70	54.06	14.55	
Mont Terri	BGC2-18	17.47	2.34	1.03	41.09	3.25	3.21	0.15	1.17	19.65	10.64	
Mont Terri	BGC2-18	12.00	1.42	0.97	41.38	3.13	3.37	0.24	1.24	24.81	11.44	
Mont Terri	BGC2-17	8.59	0.76	0.86	41.60	4.89	4.30	0.29	1.16	25.96	11.60	
Mont Terri	BGC2-15-1-oben	6.04	0.78	1.49	36.79	3.08	2.80	0.18	1.04	31.97	15.83	
Mont Terri	BGC2-15-1-unten	22.66	0.88	2.05	38.31	2.90	3.17	0.10	0.75	17.15	12.05	
Mont Terri	BGC2-15-2-oben	6.17	1.01	1.37	35.72	2.71	3.04	0.21	1.24	32.25	16.29	
Mont Terri	BGC2-15-2-unten	7.60	1.62	1.93	34.06	2.43	3.06	0.16	0.95	32.85	15.34	
Mont Terri	1756_BGC2_17_01	41.05	0.59	1.25	32.90	1.91	2.56	0.06	3.02	12.29	4.36	Y

The table presents bulk rock composition in units of volume percent and porosity of samples used to assess the relationship between bulk density and composition. The "composition" matrix Y is the response matrix that was used in the linear regression model

Table 4 The coefficients obtained for the linear models

	Calcite	Dolomite	Siderite	Quartz	Albite	K-Fsp	Pyrite	C (org)	Clay minerals	Porosity
Intercept	− 411.51	− 11.84	− 8.88	− 273.95	− 20.52	− 11.25	5.41	7.46	663.05	162.03
Slope	171.80	5.43	3.92	122.81	9.32	5.77	− 2.09	− 2.48	− 254.18	− 60.30
R-squared	0.75	0.04	0.10	0.30	0.20	0.04	0.32	0.08	0.60	0.96

The third row contains the coefficients of determination related to each linear regression

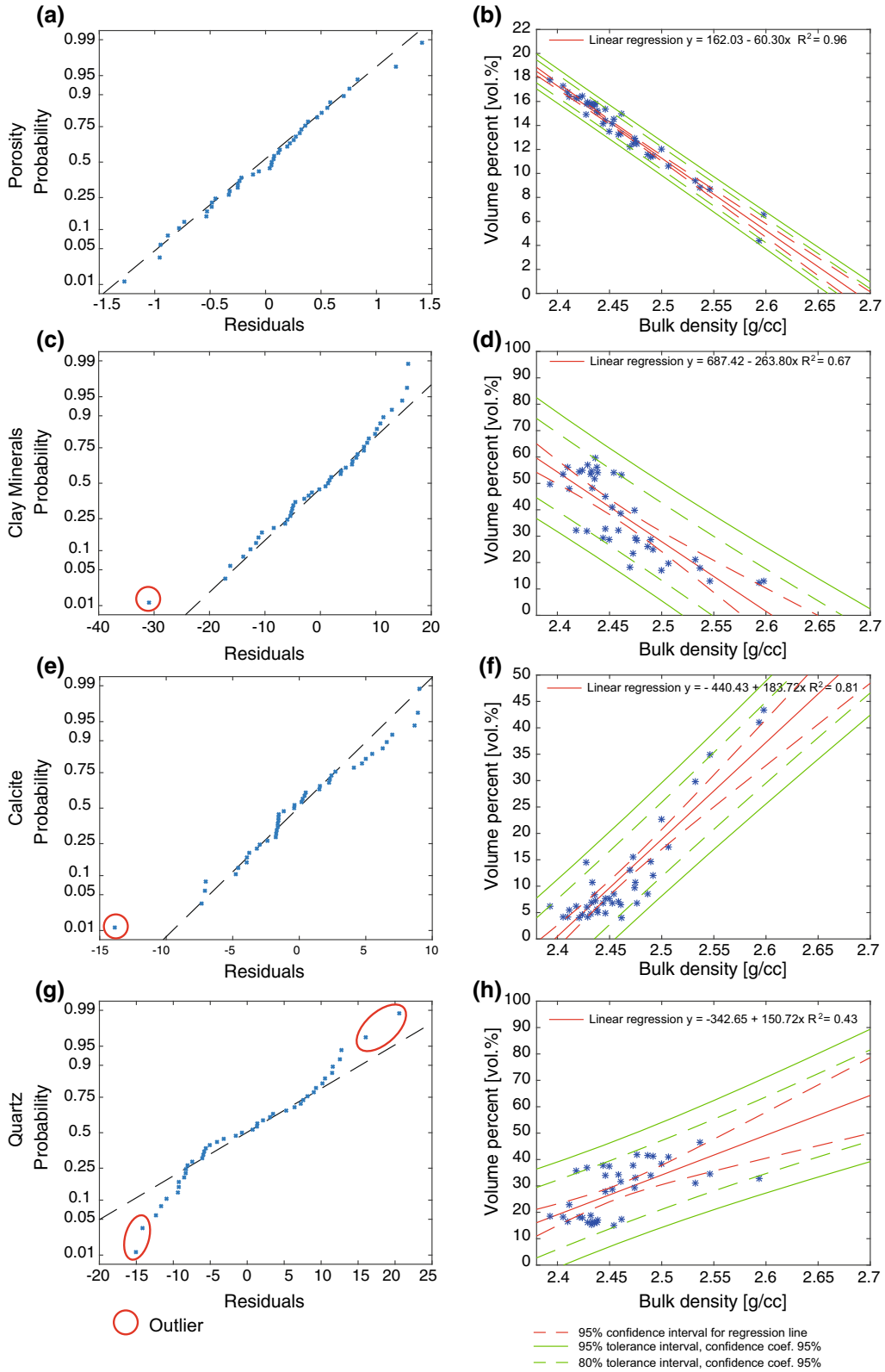
(a)
Porosity Probability
Residuals
(b)
Linear regression y = 162.03 - 60.30x R2 = 0.96
Volume percent [vol.%]
Bulk density [g/cc]
(c)
Clay Minerals Probability
Residuals
(d)
Linear regression y = 687.42 - 263.80x R2 = 0.67
Volume percent [vol.%]
Bulk density [g/cc]
(e)
Calcite Probability
Residuals
(f)
Linear regression y = - 440.43 + 183.72x R2 = 0.81
Volume percent [vol.%]
Bulk density [g/cc]
(g)
Quartz Probability
Residuals
Outlier
(h)
Linear regression y = -342.65 + 150.72x R2 = 0.43
Volume percent [vol.%]
Bulk density [g/cc]
95% confidence interval for regression line
95% tolerance interval, confidence coef. 95%
80% tolerance interval, confidence coef. 95%

Table 5 Improved coefficients obtained for linear regression models after the outliers were removed

	Calcite	Quartz	Clay minerals	Porosity
Intercept	− 440.43	− 342.65	687.42	162.03
Slope	183.72	150.72	− 263.80	− 60.30
R-squared	0.81	0.43	0.67	0.96

The third row contains the coefficients of determination related to each linear regression

responses. Whether residuals are normally distributed or not can be assessed with the help of normal probability plots, in which residuals should plot more or less on a straight line. Figure 7 shows that most residuals are close to a straight line, which backs the use of a linear regression. It is common practice to exclude small parts in the data, which have a large impact on the fitting procedure that is based on least squares. Here, data points that are not close to the straight line are no longer taken into account. No more than four data points were eliminated and the linear relationships were recalculated (Fig. 7).

As can be seen in Table 5, the exclusion of a single data point increases the value of r-squared. In Fig. 7, the 95% confidence intervals related to the regression lines are narrow and it is not possible to draw horizontal lines within the limits of the these intervals. This suggests that the mean content of clay minerals, calcite and quartz as well as porosity in Opalinus Clay are indeed systematically related to density and that the relationship between density and mineral contents or porosity can be considered linear. Note, that the confidence interval of the regression line is a measure for the uncertainty (or expected data range) of a mean value of a certain property (e.g. mean porosity of Opalinus Clay) and must not be confused with the uncertainties related to an individual value. The expected uncertainties related to an individual value can be addressed with the help of tolerance intervals. Tolerance intervals have been calculated for the relationships between densities and mineral contents or porosity (green lines in Fig. 7). In case of porosity we can be 95% sure that an interval of $\sim \pm 1.5$ vol% around the mean porosity predicted by the regression line covers about 95% of the porosity values. In case of the clay mineral content and for the same confidence and tolerance values, the interval is $\sim \pm 25$ vol% around the mean value, which is quite a considerable uncertainty. If we accept that the interval covers 80% of the values, the interval narrows to $\sim \pm 15$ vol% around the predicted mean value. The tolerance interval of the linear relationships between density and the contents of clay minerals, calcite and quartz are still too large. To reduce the interval, more data must be included.

The density calibration and the linear regression models allow the calculation of cross sections, which show, for example, the distribution of density, porosity and clay mineral content along a drill core (Fig. 8).

Of course also mineralogy and porosity profiles can be calculated from density calibrated CT numbers. Thereby, the mean density is calculated for each image plane, which is oriented parallel to the bedding plane (Fig. 9). The mean density is then used in combination with the linear regression models to calculate the porosity and contents of clay minerals, calcite and quartz (Fig. 9). Strictly speaking, the calculation of porosity or mineral contents from the above linear regressions for a given density yields mean values, which would be obtained from repeated measurements of samples. The confidence interval related to these mean values is narrow but does not provide information about the expected value range for a single sample that was taken at specific locality. Therefore, we calculated the tolerance interval, which can also be thought of as a prediction interval. This interval is the same as the one that was calculated for the linear regression models and is based on the available data set with the relationships between density and composition. Referring to Fig. 9 it is predicted that with 95% confidence at least 80% of the measured porosities and mineral contents of samples with a certain mean density would fall within these intervals.

5 Discussion

The overall objective of this study is to present a methodological approach that allows to predict the rock composition and porosity of Opalinus Clay based on XCT images and on drill core scale. The presented density calibration and the linear relationships between density and rock composition will be continuously improved by the inclusion of new data. This reduces the still partially high uncertainty in the prediction of the rock composition. Apart from the

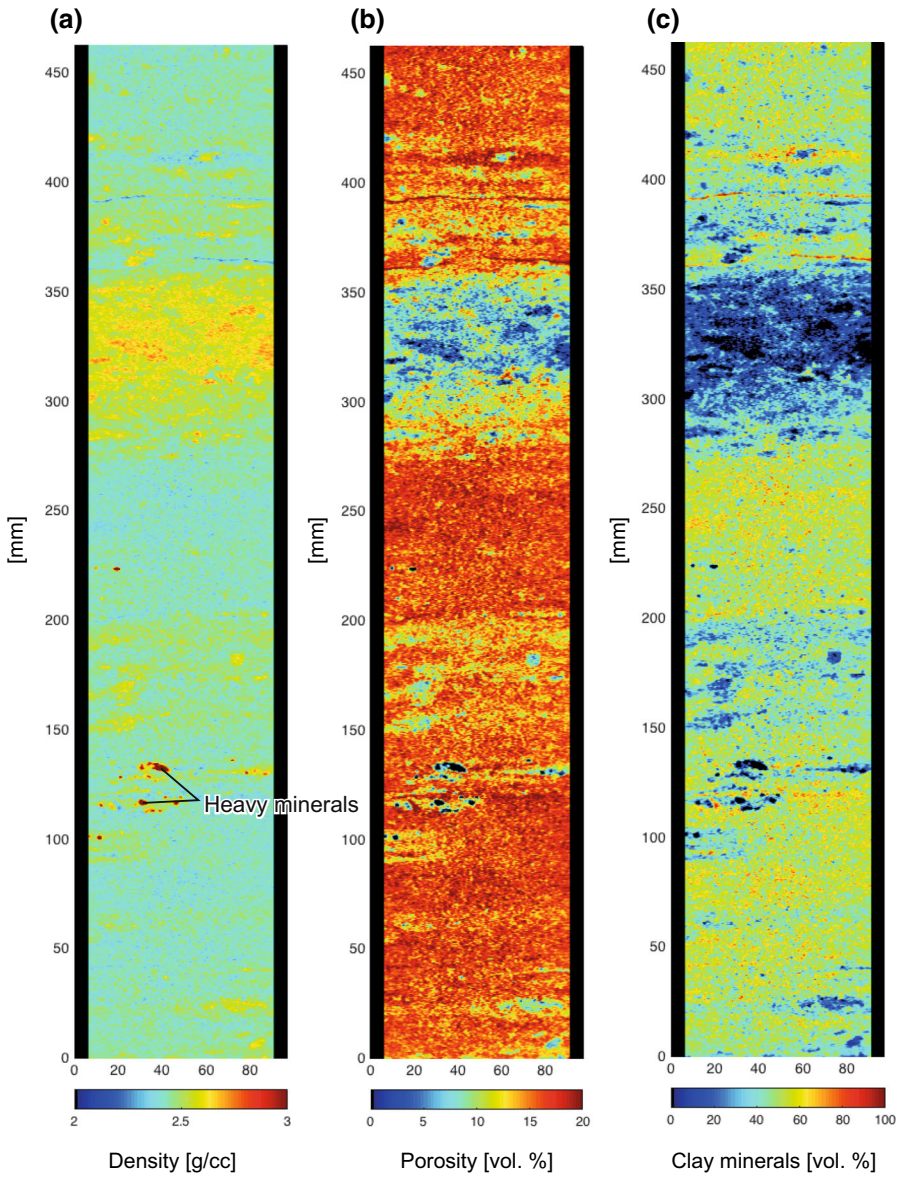

Fig. 8 Cross-sections showing the **a** bulk density distribution, **b** distribution of porosity and **c** distribution of the clay content along an Opalinus Clay drill core (BGC2-14)

presentation of the method, the presented results give an insight into the systematics of the Opalinus Clay composition.

A question that arises is whether there is a justification to combine standard samples, consisting of a single homogenous material, and samples consisting of mineral grains with different attenuation coefficients to establish a relationship between CT number and bulk density. If only the standard samples and the air were used to determine the relationship between density and CT number, this linear relationship would systematically overestimate the bulk density measured in the laboratory by up to 3%. This is probably due to the fact that the composition and structure of the standard material is not comparable to that of the clay rock. In the presented relationship between density and CT number, the specific properties of the material is taken into account by considering clay samples with known density and CT numbers. A very similar behavior was also observed for wood (see De Ridder et al. 2011 and references therein). It should also be noted that in the density range important to us, the presented relationship lies almost exactly between the one presented by Ashi

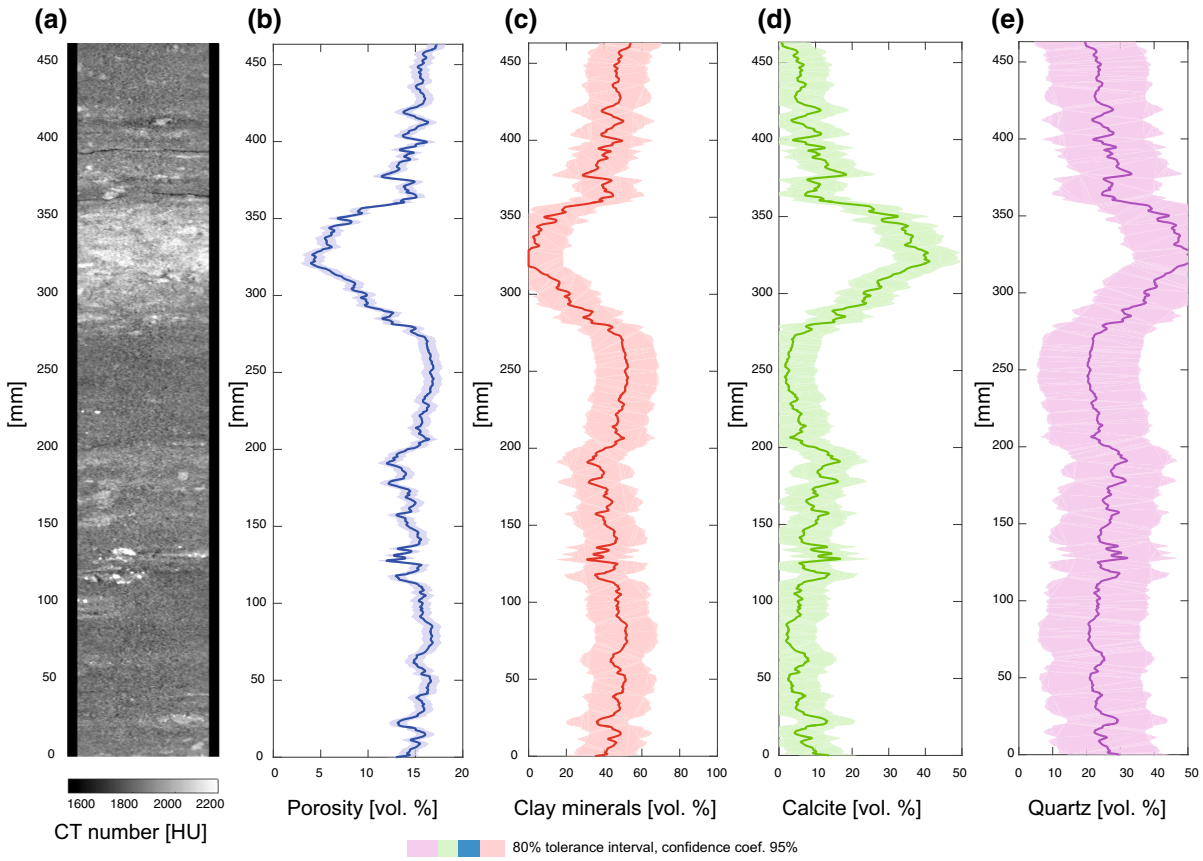

Fig. 9 **a** Cross-section showing the original distribution of CT numbers and predicted profiles: **b** porosity, **c** clay mineral content, **d** calcite content and **e** quartz content along an Opalinus Clay drill core (BGC2-14). The shaded area marks the tolerance interval (see text for further explanations)

(1995) and that of Gupta et al. (2018) (Fig. 6). These two studies also worked with geomaterials, with the calibration of Ashi (1995) based on bentonite samples with different densities. All Bentonite samples had a lower density than the clay rock samples. Gupta et al. (2018) used acryl, granite, sandstone and wood as standard material to density calibrate the CT numbers.

It is clear that the density variations of a multi-phase sedimentary rock can hypothetically be produced by an infinite number of compositional combinations. However, the prerequisite for this is that there is no systematics in the composition of this rock. Fortunately, Opalinus Clay has such a systematic, which is largely controlled by its microstructural properties. Clay rocks are often considered as two-component systems consisting of a porous clay matrix and non-clay minerals (e.g. Revil and Cathles 1999). This approach is also supported by microstructural investigations (Keller et al. 2013). If so, the porosity and clay mineral content should vary with density in the same way, which is indeed the case, because they are structurally connected. Specifically, both porosity and clay mineral content decrease with increasing bulk density (Fig. 7). In contrast, the content of quartz and calcite increases with increasing density.

As for the accuracy of predictions, predicting the composition of an individual sample at a given location is different from the prediction of the expected mean composition that would result from repeated measurements and to which the linear regression line refers. For the prediction of the composition of an individual sample from the established linear regression models, it makes sense to specify an expected value range in the form of a tolerance interval. This interval covers a certain proportion of the expected values with a certain level of confidence. Using the size of this interval as measure for the prediction accuracy it turned out that

the prediction of porosity may be considered robust. The prediction of the clay mineral content, the calcite and quartz content is still uncertain (large tolerance intervals) and needs to be improved (Fig. 7). For this purpose, the number of samples must be increased, i.e. further samples must be measured in the laboratory.

6 Conclusion

The use of a medical X-ray scanner allowed a fast, non-destructive and cost-effective imaging of clay rock drill cores with diameters of about 10 cm. For this sample size the voxel size of the acquired image data is larger than the grain and pore sizes of clay rocks. Individual grains or pores therefore cannot be resolved, and the CT values of the voxels are controlled by the respective volume fraction of the different phases and pores in the voxel volume. Knowing the quantitative relation between image CT-values (grey values) and rock density allows for a continuous determination of the rock density along the drill cores. The same also applies for the distribution of rock mineral composition, although a larger number of reference samples is required for satisfactory correlation. Porosity and mineralogy distribution as documented in XCT cross-sections are of valuable assistance in guiding sub-sampling intervals and interpretation of results (upscaling) of laboratory testing.

Acknowledgements Bulk rock mineralogy and bulk wet density data was provided by University of Bern. The authors acknowledge fruitful discussions and exchanges with Prof. M. Mazurek.

References

Ashi J (1995) CT scan analysis of sediments from Leg 146. In: Carson B, Westbrook GK, Musgrave RJ, Suess E (eds) Proceedings of the ocean drilling program, scientific results, vol 146 (Pt. 1), pp 191–199

Ashi J (1997) Computed tomography scan image analysis of sediments. In: Shipley TH, Ogawa Y, Blum P, Bahr JM (eds) Proceedings of the ocean drilling program, scientific results, vol 156, pp 151–159

Bossart P, Thury M (2008) Mont Terri Rock Laboratory: project, programme 1996–2007 and results. Reports of the Swiss Geological Survey, No. 3

Brabant L, Pauwels E, Dierick M, Van Loo D, Boone MA, Van Hoorebeke L (2012) A novel beam hardening correction method requiring no prior knowledge, incorporated in an iterative reconstruction algorithm. NDT&E Int 51:68–73

De Ridder M, Van den Bulcke J, Vansteenkiste D, Van Loo D, Dierick M, Masschaele B, De Witte Y, Mannes D, Lehmann E, Beeckman H, Van Hoorebeke L, Van Acker J (2011) High-resolution proxies for wood density variations in *Terminalia superba*. Ann Bot 107:293–302

Giger SB, Ewy RT, Favero V, Stankovic R, Keller LM (2018) Consolidated-undrained triaxial testing of Opalinus Clay: results and method validation. Geomech Energy Environ 14:16–28

Gupta LP, Tanikawa W, Hamada Y, Hirose T, Ahagon N, Sigihara T, Abe N, Nomura Y, Wu HY, Lin W, Kinoshita M, Yamada Y, Expedition NGHP, 02 JAMSTEC Science Team (2018) Examination of gas hydrate-bearing deep ocean sediments by X-ray computed tomography and verification of physical property measurements of sediments. Mar Pet Geol. https://doi.org/10.1016/j.marpetgeo.2018.05.033

Jovanovic Z, Khan F, Enzmann F, Kersten M (2013) Simultaneous segmentation and beam-hardening correction in computed microtomography of rock cores. Comput Geosci 56:142–150

Keller LM, Schuetz P, Gasser P, Holzer L (2013) Pore-space relevant for gas-permeability in Opalinus Clay: statistical analysis of homogeneity, percolation and representative volume element. J Geophys Res: Solid Earth 118:2799–2812. https://doi.org/10.1002/jgrb.50228

Khan F, Enzmann F, Kersten M (2016) Multi-phase classification by least-squares support vector machine approach in tomography images of geological samples. Solid Earth 7:481–492

Mazurek M, Waber HN, Maeder UK, Gimmi T, de Haller A, Koroleva M (2012) Geochemical synthesis for the Effinger member in Boreholes at Oftringen, Goesgen and Kuettigen, Nagra technical report NTB 12-07. Nagra Weinfelden, Switzerland

Mees F, Swennen R, Van Geet M, Jacobs P (2003) Applications of X-ray computed tomography in the geosciences. Geological Society, London, vol 215. Special Publications, pp 1–6

Nagra (2002) Projekt Opalinuston—Synthese der geowissenschafftlichen Untersuchungsergebnisse. Entsorgungsnachweis für abgebrannte Brennelemente, verglaste hochaktive sowie langlebige mittelaktive Abfälle. Nagra technical report NTB 02-03, Nagra Weinfelden, Switzerland

Revil A, Cathles LM (1999) Permeability of shaly sands. Water Resour Res 35:651–662

Schlüter S, Sheppard A, Brown K, Wildenschild D (2014) Image processing of multiphase images obtained via X-ray microtomography: a review. Water Resour Res 50:3615–3639

Taud H, Martinez-Angeles R, Parrot JF, Hernandez-Escobedo L (2005) Porosity estimation method by X-ray computed tomography. J Pet Sci Eng 47:209–217

Wallis WA (1951) Tolerance intervals for linear regression. In: Neyman J (ed) Second Berkeley symposium on mathematical statistics and probability. University of California Press, Los Angeles, pp 43–51